Environmental Sciences Europe

RESEARCH

Open Access

Environmental significance of the interaction between titanium dioxides and soil solutions

Karolina Solymos[1,2], Izabella Babcsányi[2], Badam Ariya[1], Tamás Gyulavári[1], Áron Ágoston[1,3], Ákos Kukovecz[1], Zoltán Kónya[1] and Zsolt Pap[1,4,5*]

Abstract

Nanotechnology, especially in the field of photocatalysis, has witnessed rapid advancements, with titanium dioxide being one of the most widely used photocatalysts. As the use of products containing photoactive nanomaterials increases, concerns have arisen regarding their potential release into the environment over time. This release can impact soil, groundwater, and surrounding ecosystems, resulting in nanoparticles being dispersed in water and eventually depleted from the system. This study aimed to investigate how different soil solutions affect the structural, textural properties, and photocatalytic activity of titanium dioxide-based, commercial reference Evonik Aeroxide P25. The Regosol soil solution, characterized by acidic pH, low ionic content, and high organic matter content, induced nanoparticle aggregation and bandgap changes. In addition, the acidic pH hindered the adsorption process, potentially affecting the photocatalytic processes. In contrast, the Chernozem soil solution, with slightly alkaline pH, high ionic content, and low organic matter content, did not significantly alter the morphology or structure of the material. However, various organic compounds were absorbed on the surface, reducing the availability of active sites. The study highlights the importance of understanding the influence of soil solutions on nanomaterials, as it impacts their properties and environmental risks. Results show that the material is still activated, i.e., it can exert its photoactive effect on the environment. This sheds light on the challenges posed by nanoparticles in soil, particularly in terms of their toxicity and consequences for the surrounding ecosystems. The study underlines the need for further research in this area to assess potential risks and optimise the use of nanomaterials in environmental remediation.

Keywords Titania, Soil solution, Chernozem, Regosol, Photocatalysis

Background

The widespread use of TiO_2 in nanotechnology can be attributed to its cost-effectiveness and photochemical stability [1]. TiO_2 has a wide bandgap, enabling it to absorb ultraviolet (UV) light and generate electron–hole pairs efficiently. Electrons and holes can participate in reduction and oxidation reactions, facilitating the degradation of organic pollutants through direct oxidation or the generation of reactive free radicals, such as hydroxyl radical (•OH) [2]. Due to its outstanding efficiency, TiO_2 nanoparticles (NPs) have gained widespread success in practical applications and are commercially produced on a large scale. Estimates suggest that nanosized TiO_2 will dominate the market by 2025, with a global production of 14 million tons [3, 4].

*Correspondence:
Zsolt Pap
pzsolt@chem.u-szeged.hu
[1] Department of Applied and Environmental Chemistry, University of Szeged, Rerrich Sqr. 1, Szeged U6720, Hungary
[2] Department of Geoinformatics, Physical and Environmental Geography, University of Szeged, Egyetem Str. 2-6, Szeged U6722, Hungary
[3] Department of Physical Chemistry and Materials Sciences, University of Szeged, Rerrich B. Sqr.1, U6720 Szeged, Hungary
[4] Institute of Interdisciplinary Research in Bio-Nano-Sciences, Babeş–Bolyai University, Treboniu Laurian Str. 42, 400271 Cluj-Napoca, Romania
[5] Centre for 3B, Babeş–Bolyai University, Clinicilor 5-7, 400006 Cluj-Napoca, Romania

A notable product in this category is Evonik's AEROXIDE® TiO_2 P-25 (P25), the most widely used commercial TiO_2 for researching photocatalytic processes, and to develop self-cleaning surfaces [5, 6]. When exposed to UV light, P25 degrades organic compounds, in which is the basic procedure for a self-cleaning surface [7, 8]. This characteristic significantly reduces the need for manual cleaning, particularly in outdoor applications, making these surfaces highly advantageous. Common applications include self-cleaning glass in architecture [9], automotive coatings, and outdoor signage [10–12].

With the increasing use of products containing photoactive nanomaterials, their erosion and corrosion over time can result in their release into the soil [13–15]. Naturally, TiO_2 NPs also can be present in soils and sediments due to the weathering and erosion of rocks containing titanium minerals [16]. The increasing presence of TiO_2 NPs in soil is raising concerns, and identifying them poses challenges due to limitations in extraction and separation methods [17]. The expected concentration of TiO_2 NPs in soil is ~ 50 $mg{\cdot}kg^{-1}$ in the European Union [18]. In the United States, sewage sludge has shown concentrations ranging from 1.8 to 6.4 $mg{\cdot}kg^{-1}$ of TiO_2 NPs, while in the UK, the concentration was found to be 305 $mg{\cdot}kg^{-1}$ [19, 20]. Moreover, various models have been developed to forecast the fate of TiO_2 NPs in the environment, and the outcomes consistently indicate a rise in their concentration over time [13, 21, 22].

In the process of entering the soil, rainfall plays a crucial role by actively interacting with the soil, facilitating the removal of TiO_2 NPs from various surfaces [23–25]. The three-phase soil dynamics occur on the surface, where TiO_2 NPs either bind to the solid phase of the soil or disperse, becoming part of the soil solution [26]. However, the interaction of TiO_2 NPs with soil solutions extends beyond surface processes. Leaching serves as another significant pathway, where water transports NPs into soil pores, especially when they are not strongly attached to soil particles [27, 28]. This underscores the potential for TiO_2 NPs to move and redistribute within the soil environment, influenced by environmental factors, such as rainfall and leaching processes. What does not bind to the surface is subsequently washed down into the deeper layers, ultimately reaching the groundwater [29, 30].

Previous studies have shed light on the behavior NPs in soil solutions and the associated mechanisms. For instance, a prior investigation shows that the enhanced stability of suspended TiO_2 concentrations, attributed to factors, such as a higher zeta potential, promotes their heightened mobility through diverse layers of the soil [31]. In the case of Ag NPs, their stability is influenced by the sorption of solutes, such as Ca^{2+} from the soil solution, where dissolved organic matter (DOM) exhibits a concentration-dependent stabilizing effect [26, 32]. Furthermore, the interaction between CuO NPs and DOM highlights that hydrophobic DOM stabilizes CuO NPs more effectively than hydrophilic DOM in the presence of Ca^{2+} [28, 33, 34].

Soils differ in composition, texture, and genetic processes. For example, the Chernozem soil (mainly found in Eastern Europe) has been characterized by the World Reference Base of Soil Resources with a mollic horizon (dark in color with an organic matter content of at least 0.6%), a depth of occurrence of at least 20 cm, and a texture of sandy–loam or loamy. Due to the organic matter content and the texture, the biological activity of Chernozem soils is high, so their crop yield is favorable too. Therefore, this soil type is usually utilized as arable land [35]. Another example is the Regosol soil type, covering approximately 2% of the continental land area on Earth, mainly including the hill slopes [36] in Northern China, the Middle East, and Eastern Europe. Regosol soils are found under natural vegetation and crops and can be characterized by high organic matter content (> 2%), sandy texture, and reddish brown color. Based on the information provided above and considering their abundance in Europe, these two soil types were chosen for the investigations.

While existing research has primarily concentrated on the impact of NPs in aquatic environments, there is a recognized gap in our understanding of their effects on soil solutions. This study contributes to this area by underscoring the importance of investigating the relationship between NPs and soil solutions. The aim is to provide valuable insights into the environmental risks associated with NPs, particularly addressing the limited knowledge about how the physicochemical properties of soil solutions influence the catalytic activity of TiO_2 NPs. Further exploration in this field is essential for developing a more comprehensive understanding of the environmental implications of these NPs.

Therefore, the aim of this study is to assess the impact of different soil solutions on the structural properties of the widely used commercial reference material, Evonik Aeroxide P25 TiO_2, with a specific focus on environmental protection considerations. Two distinct artificially prepared soil solutions, designed to replicate the characteristics of Chernozem and Regosol soils, were employed in the investigation. The study examines the interaction between these soil solutions and Evonik Aeroxide P25, emphasizing changes in photocatalytic activity as well as several structural and textural characteristics, including morphology, crystalline composition, surface features, and optical properties. By concentrating on the environmental implications, the research aims to contribute

valuable insights into how TiO_2 materials behave in different environmental conditions.

Materials and methods

Materials

The following TiO_2 NPs were used during the experiments: Evonik Aeroxide P25 (anatase:rutile = 89%:11%) was purchased from VWR, Hungary, and was used in all the experiments without prior treatment or modification. Ultra-pure Millipore Milli-Q (MQ) water was used for preparing the soil solutions. To determine the photocatalytic activities, phenol (VWR, > 99%) was used as a model pollutant.

KBr (99.0%, Millipore Sigma, Uvasol) was used to prepare the samples for infrared spectroscopy (IR). 0.1 mM and 0.01 mM NaOH and HCl were used to adjust the pH before the zeta (ζ) potential measurements. For the determination of the organic matter content (OM) of the soils, H_2SO_4 (95%, VWR) and 0.33 M $K_2Cr_2O_7$ (VWR) were used.

The samples were digested with HNO3 (65%, VWR) and HCl (37%, VWR). To determine the chemical oxygen demand (COD) of the soil solutions, 0.002 M $KMnO_4$, 0.005 M $Na_2C_2O_4$, and 0.005 M H_2SO_4 were used. Argon (VWR, > 99.99% purity) was the carrier gas for inductively coupled plasma optical emission spectrometric (ICP-OES) measurements.

For the flow injection analysis (FIA) measurements, NH_4Cl buffer (pH = 8.5) was used as a reagent to determine NO_3^-, for PO_4^{3-} determination, $SnCl_2$ and $(NH_4)_6Mo_7O_{24}$ were used. For the ion chromatography (IC) measurement, 0.5 M Na_2CO_3 was used as the eluent composition.

Soil sampling and analysis

Soil samples (10 Regosol and 10 Chernozem topsoil samples) were collected (Fig. 1) from an agricultural land near Szeged, Hungary and from a forest near Tallya, Hungary. The soil samples were taken from 0 to 20 cm depths in September 2021 and in January 2022. Sampling was performed by mixing topsoil samples from 0 to 10 cm and 10 to 20 cm layers. The soil samples were dried in air for 10 days and sieved with a 2 mm diameter sieve. Primary soil parameters such as pH, electrical conductivity (EC), total salt content, texture, and OM content were determined following the Hungarian standards (MSZ), and can be found in Supplementary information.

Soil solution extraction and analysis

Soil solutions were obtained using the methodology developed by Klitzke et al. [32] and Qiu et al. [33]. The soil solutions were prepared using Milli-Q water, applying a solid-to-solution ratio of 1:2.5. The mixtures were shaken with a tube rotator (40 rpm) for 18 h, centrifuged at 3700 rpm for 30 min and subsequently filtered with a 0.45 µm cellulose nitrate membrane.

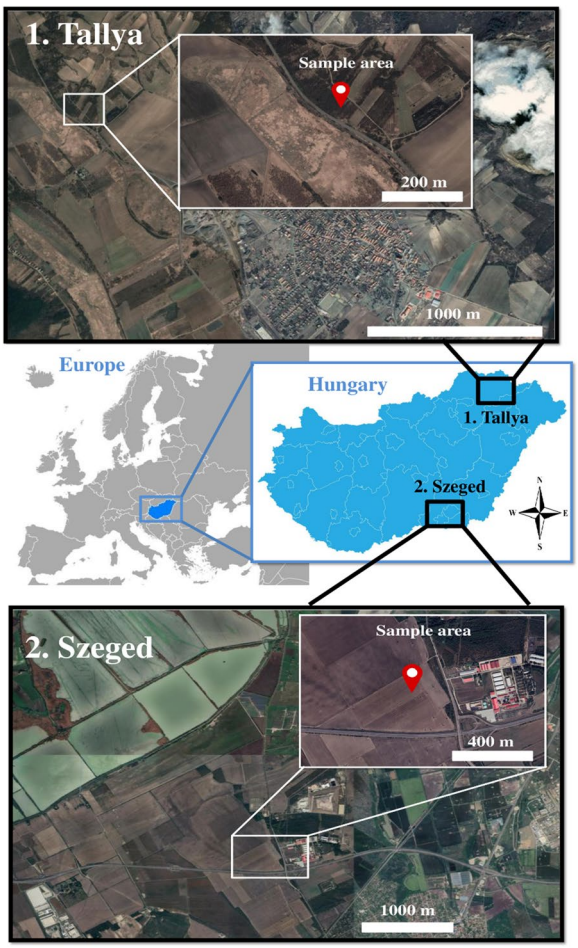

Fig. 1 Location of the sampling areas

The pH of the soil solution was measured with a digital pH meter (Inolab pH 720), while the EC was determined using a conductivity meter (Orion 3-Star, Thermo Electron Corporation). COD values were determined following the Hungarian Standards (details in the Supplementary information).

Ionic strengths (Eq. 1) were calculated from the EC results [33].

$$\begin{aligned} &IS = EC \cdot 0.0127 \\ &IS - \text{ionic strength}\left(\text{mol} \cdot \text{L}^{-1}\right) \\ &EC - \text{electrical conductivity}\left(\text{mS} \cdot \text{cm}^{-1}\right) \end{aligned} \quad (1)$$

The concentration of major elements (Na, K, Ca, Mg) was measured ICP-OES (Perkin Elmer Optima 7000DV).

Foss FIA Star 5000 spectrometer was using for the determination of NO_3^-, and PO_4^{3-} content. F^-, Cl^-, NH_4^+ and SO_4^{2-}concentrations were determined using a Dionex ICS^{-1}600 ion chromatograph.

Characterization of nanomaterials

X-ray diffraction (XRD) patterns were recorded with a Rigaku Miniflex II diffractometer equipped with a graphite monochromator using Cu-Kα radiation (λ = 1.5406 Å). Data points were taken in the 2θ = 20–40° range at a scan speed of 1 min^{-1}. Primary crystallite sizes were calculated using the Scherrer equation [37].

The morphology of the samples was characterized with a Hitachi S-4700 Type II scanning electron microscope (SEM) after coating them with gold NPs (< 10 nm).

An IR spectrometer (Bruker Equinox 55) was used to examine the changes on the surface of TiO_2 NPs. The samples and KBr powder were pressed into pellets, and the IR spectra were recorded with a resolution of 2 cm^{-1}. To determine the bandgap values and also the color changes following the interaction with soil extracts JASCO-V650 spectrophotometer with an integration sphere (ILV-724) was used to record the diffuse reflectance spectra (DRS) of the samples (λ = 220–800 nm). $BaSO_4$ was used as a reference, and the bandgap energy was calculated based on the Kubelka–Munk method [38].

The ζ potential of the NPs was determined with a Horiba SZ-100 Nanoparticle Analyzer (Retsch Technology GmbH, Germany). The measurements were performed in a carbon electrode cell. The ζ potential values were determined using the Smoluchowski model. The measured dispersion concentration was 0.001 w/v%.

The photocatalytic activity of P25 NPs was evaluated by phenol degradation experiments. P25 NPs (1 g·L^{-1}) were added to a phenol solution (c_0 = 0.1 mM), and the suspension was sonicated for 10 min. Then, the suspension was poured into a double-walled glass vessel (V = 100 mL) surrounded by six fluorescent UV tubes (Vilber–Lourmat T-6L UV-A, 6W). To reach adsorption–desorption equilibrium, we stirred the suspension in the dark for 10 min before switching on the lamps. The concentration of phenol was followed by an HPLC system consisting of a Merck Hitachi L-4250 UV–Vis detector and a Merck Hitachi L-7100 low-pressure pump (0.7 cm^3·min^{-1} flow rate; detection at 210 nm) using a 50:50 (v/v) methanol/water mixture as an eluent.

Soil solution experiments

The ten Chernozem and ten Regosol pre-prepared soil solutions were merged, and throughout the experiments, a singular Chernozem and a Regosol representative homogeneous sample was employed. The P25 NPs stock suspension (10 g·L^{-1}) was prepared using Milli-Q water under ultrasonication (10 min). The final concentration of the P25 NPs in the soil solutions was 1 g·L^{-1} after blending. The established suspension concentration was determined based on experimental reproducibility and typical catalytic applications [6, 7]. Subsequent to adding the P25 stock suspension to the soil solution, the resultant suspension underwent mixing with a magnetic stirrer under light protection. Following a 1-, 4- and 24-h interaction between P25 NPs and the soil solutions, the suspensions underwent centrifugation for 10 min at 3700 RPM (1531 RCF). A schematic representation of the steps of the methodology is shown in Additional file 1: Fig. S1.

List of abbreviations the investigated samples were coded as follows: *P25_REF:* pure/reference P25; *P25_AP:* P25 after phenol degradation; *P25_REG_1:* P25 after 1-h interaction with Regosol soil solution; *P25_REG1_AP:* P25 after 1-h interaction with Regosol soil solution; *P25_REG_4:* P25 after 4-h interaction with Regosol soil solution; *P25_REG4_AP:* P25 after 4-h interaction with Regosol soil solution*; P25_REG_24:* P25 after 24-h interaction with Regosol soil solution; *P25_REG24_AP:* P25 after 24-h interaction with Regosol soil solution*; P25_CH_1:* P25 after 1-h interaction with Chernozem soil solution; *P25_CH1_AP:* P25 after 1-h interaction with Chernozem soil solution and phenol degradation; *P25_CH_4:* P25 after 4-h interaction with Chernozem soil solution; *P25_CH4_AP:* P25 after 4-h interaction with Chernozem soil solution and phenol degradation; *P25_CH_24:* P25 after 24-h interaction with Chernozem soil solution; *P25_CH24_AP:* P25 after 24-h interaction with Chernozem soil solution and phenol degradation.

Results and discussion

Evonik aeroxide P25 characterization before immersion in soil solution

Before immersion in soil solutions, the properties of P25 was investigated. The SEM micrograph shows that the P25 sample contained particles of different shapes due to its polycrystalline structure (Fig. 2a). The XRD pattern shows that it contained anatase and rutile phases based on the diffraction peaks at 25.6° and 38.0° for the former and at 27.2° and 36.1° for the latter (Fig. 2b). The average crystallite size of P25 was calculated to be 24.8 nm based on the Scherrer equation. Due to their diminutive size, small particles exhibit ease of suspension in aqueous media [39]. In addition, this characteristic also implies a propensity for these particles to diffuse into cell membranes, potentially causing harm to living organisms [40–43]. The excitability of the material, such as P25, is determined by its bandgap, which, in the case of P25, is in the UV region, specifically in the UV-A range, and sunlight contains a significant amount of UV-A radiation. Based on the DR spectrum of P25 (Fig. 2c), we found that

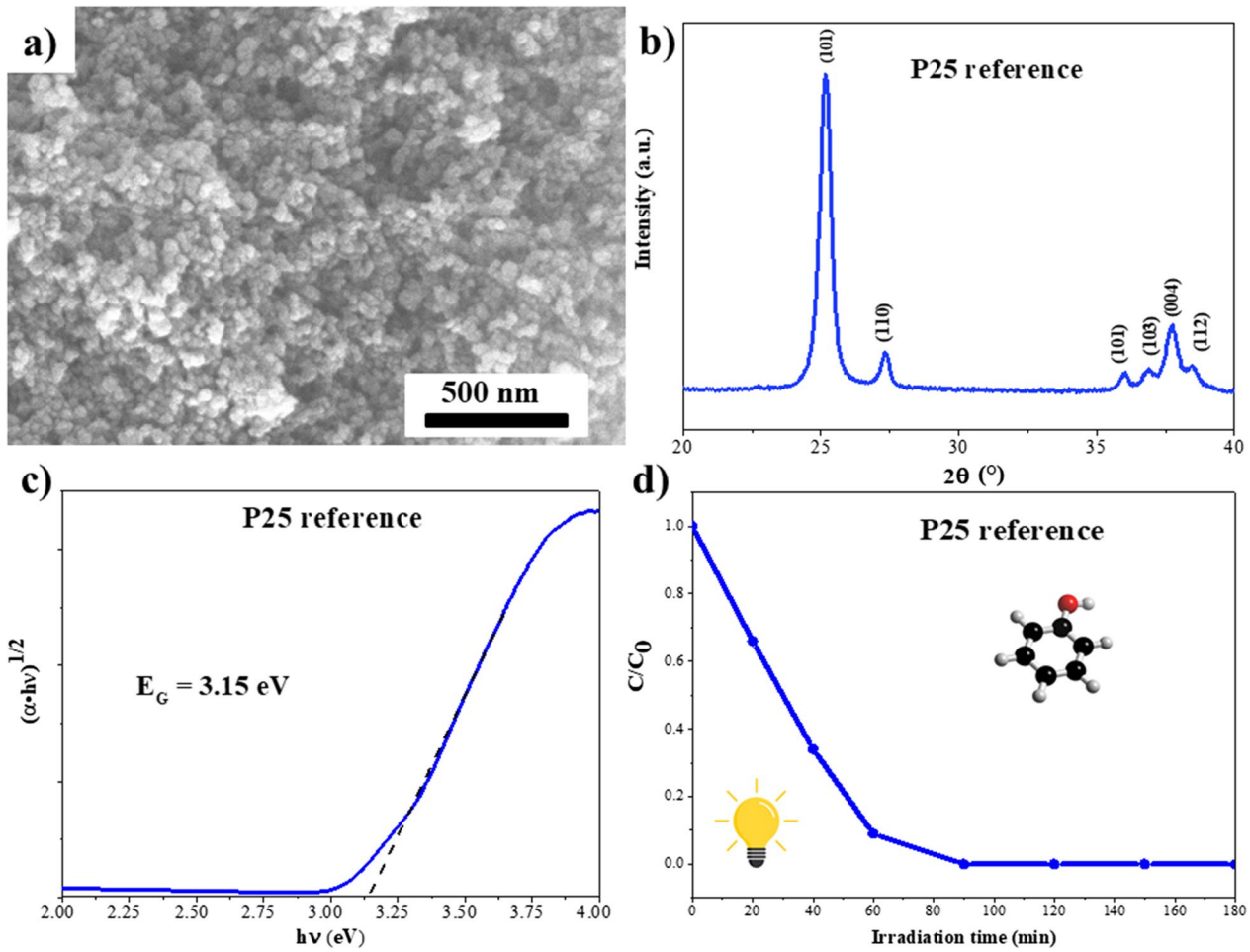

Fig. 2 **a** SEM-micrograph, **b** XRD-pattern, **c** DR spectrum (with bandgap evaluation), and **d** phenol degradation curve of P25 TiO_2

the bandgap was 3.15 eV, which is consistent with literature data [44]. Lastly, the degradation of phenol is highly efficient, even at a concentration as low as 0.1 mM, as depicted in its overall properties (Fig. 2d). This implies its capability to degrade any organic matter, potentially leading to a significant local concentration change upon release into the environment. This high catalytic activity can be attributed to the (i) synergistic effect between the anatase and rutile phases and their different surface energies [45], (ii) relatively high specific surface area, resulting in many active sites on the surface [46], and (iii) efficient excitability [47].

Properties of soil solutions and their possible effects on the behavior of TiO_2 NPs

The pH, IS, COD, and inorganic ion content of regosol and chernozem soil solutions were investigated (Table 1, Additional file 1: Tables S2, S3).

The pH values of the soil solution were different: the average pH of the Regosol soil solution (REG) was ~ 4.95

Table 1 Physicochemical parameters of soil solutions

Parameters		REGOSOL soil solution (REG)	CHERNOZEM soil solution (CH)
pH		4.95 ± 0.1	7.74 ± 0.2
IS ($mmol \cdot L^{-1}$)		1.99 ± 0.1	3.96 ± 0.1
COD	$mg \cdot L^{-1}$	165 ± 1.2	20.9 ± 0.4
Na^+		2.61 ± 0.5	8.31 ± 0.1
K^+		38.35 ± 0.8	5.59 ± 0.2
Ca^{2+}		32.62 ± 0.9	57.61 ± 0.1
Mg^{2+}		9.84 ± 0.2	6.60 ± 0.0
NO_3^-		21.55 ± 0.1	74.61 ± 0.7
PO_4^{3-}		1.33 ± 0.1	0.98 ± 0.09
NH_4^+		1.39 ± 0.3	0.33 ± 0.1
F^-		0.13 ± 0.02	0.62 ± 0.04
Cl^-		3.45 ± 0.05	9.61 ± 0.2
SO_4^{2-}		1.73 ± 0.3	3.2 ± 0.1

(acidic), while that of the Chernozem soil solution (CH) was ~ 7.74 (slightly alkaline). It is known that pH significantly influences the isoelectric point (IEP) and ζ potential of catalysts.

Significant differences were observed between the COD concentrations of the soil solutions. The COD of the CH was 20.9 $mg{\cdot}L^{-1}$, while for the REG, a much higher value (165 $mg{\cdot}L^{-1}$) was measured. The significant differences between pH and COD values are due to areal characteristics. Regosol soil samples (the basis of REG) were collected from forest areas with high biomass turnover and soil acidification by microbial decomposition products. COD values also represent the organic matter content of aqueous media [48]. The high organic matter content strongly affects the photocatalytic activity of P25, because various organic compounds can adsorb onto its surface, hindering access to its active sites [49]. This impedes the interaction between the photocatalyst and the target pollutants or substrates. In addition, organic molecules may compete with the target pollutants for adsorption onto the P25 surface. If the organic molecules have a higher affinity for the surface, they can effectively displace the target pollutants, diminishing the photocatalytic activity towards those pollutants [50].

The behavior of the P25 photocatalyst can be affected the presence of specific ions too, so their concentrations in soil solutions were measured too. Na^+ and Ca^{2+} concentrations were low for REG and high for CH. Various authors reported increased sedimentation and aggregation at similar values for TiO_2 NPs in water [39, 51, 52]. The K^+ and Mg^{2+} concentrations in the REG were much higher than in the CH, which could be due to the geochemical characteristics (e.g. bedrock) the area from which the Regosol soil samples were collected.

Differences in the anion concentrations were also significant. The concentration of NO_3^- in the REG was 21.55 $mg{\cdot}L^{-1}$, while in the CH, a much higher value (74.61 $mg{\cdot}L^{-1}$) was measured. Based on literature data, even 50 $mg{\cdot}L^{-1}$ NO_3^- the ζ potential of TiO_2 exhibited a gradual decrease, eventually nearing zero, leading to a subsequent increase in aggregate size [53]. Similar PO_4^{3-} concentrations were measured for the two types of soil solutions. A previous study shows, that even at millimolar concentrations, PO_4^{3-} decreases the activity of TiO_2, because it strongly adsorbs onto the TiO_2 surface [54]. The differences were significant for NH_4^+ values of CH (0.33 $mg{\cdot}L^{-1}$) and REG (1.39 $mg{\cdot}L^{-1}$) samples. The higher value for the latter can be associated with the intensive microbial activity in the area from which the soil samples were collected [55]. The NH_3 content has similar effect to the TiO_2 activity as PO_4^{3-} [56]. Finally, F^-, Cl^-, and SO_4^{2-} ions were considered. Significant differences were observed for the first two, while for SO_4^{2-}, the difference was not as notable. These ions can also bind to the active sites of catalysts, blocking access for reactant molecules and thus hindering photocatalytic reactions [57–59]. However, it is crucial to acknowledge that the effect of SO_4^{2-} content on activity is highly dependent on the specific synthesis method employed. Different methods can lead to variations in the material's structure, composition, and properties, which in turn affect its reactivity or and can increase the photocatalytic activity of the material [60]

Morphology, crystal structure, particle size, and optical properties of P25 after immersion in soil solution

As the next step, the effect of soil solutions on the properties of P25 TiO_2 was investigated. Based on the XRD patterns in Fig. 3, the crystal structure of P25 did not change significantly (there were no changes in the intensity and width of the peaks) after its immersion in the soil solutions. The stability of the crystal structure suggests that if P25 NPs are released into the environment, they are likely to retain their properties and key applicability. SEM micrographs show that the morphology of NPs did not change; however, the aggregation of NPs can be observed: in the case of REG already after 1 h of interaction, and in the case of CH after 24-h interaction time (Fig. 4). This can be correlated to the organic matter content of REG, because various organic compounds with different ions can adsorb to the surface, which induces aggregation. Due to this, the particles sediment faster [61, 62].

Optical changes were also observed following the interaction of P25 with CH and REG. Figure 5 shows significant spectral differences between the samples in the visible region (differently colored samples). This can indicate potential adsorption of reflectance onto the surface and alterations in attached materials affecting both color and semiconductor properties (Fig. 5a, b). However, it is important to note that even if the color changes, that may not result in significant changes in its photocatalytic properties [63].

Figure 5c summarizes the bandgap values of the P25 samples. The bandgaps decreased (suffered a red shift) by 0.15 eV and 0.5 eV after interaction with CH and REG, respectively. However, the bandgaps within the soil solution types did not show significant variations over different interaction times, with a maximum difference of 0.12 eV. Interestingly, minimal increases were observed for almost all samples after phenol degradation, compared to those interacting with soil solutions (e.g., P25_CH_4 has 3.0 eV, while P25_CH4_AP has 3.1 eV).

We excluded the possibility that the ions in the soil solutions caused the changes in the bandgaps. Although transition metals (e.g., Fe^{3+}) can cause such changes, this

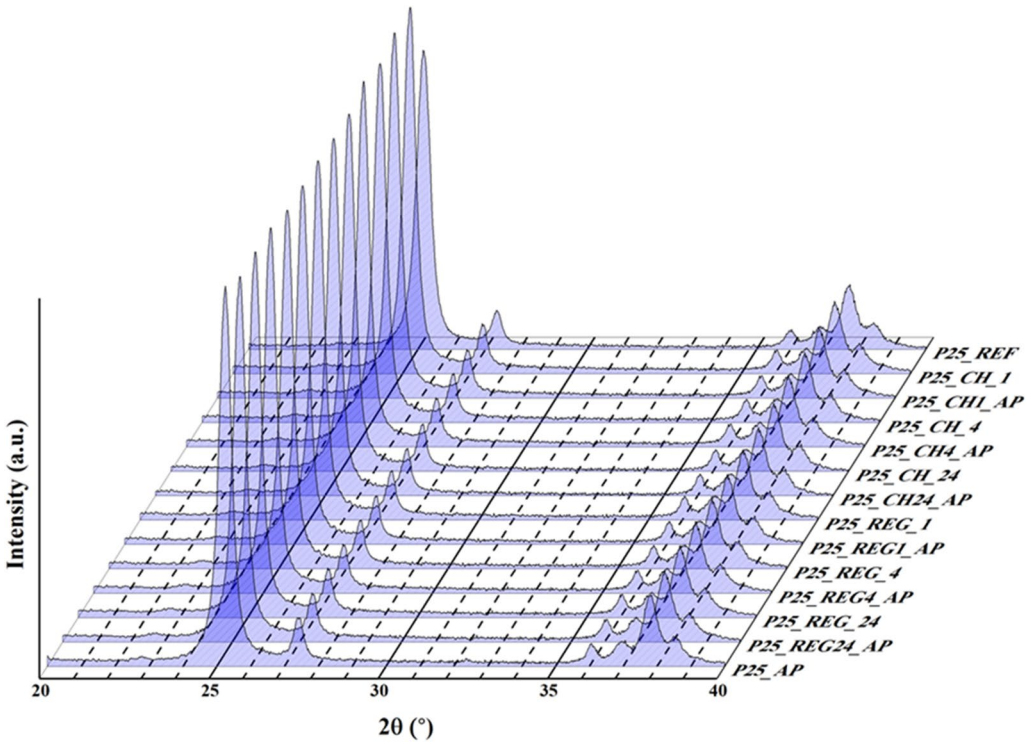

Fig. 3 XRD patterns of P25 samples before and after interaction with soil solutions

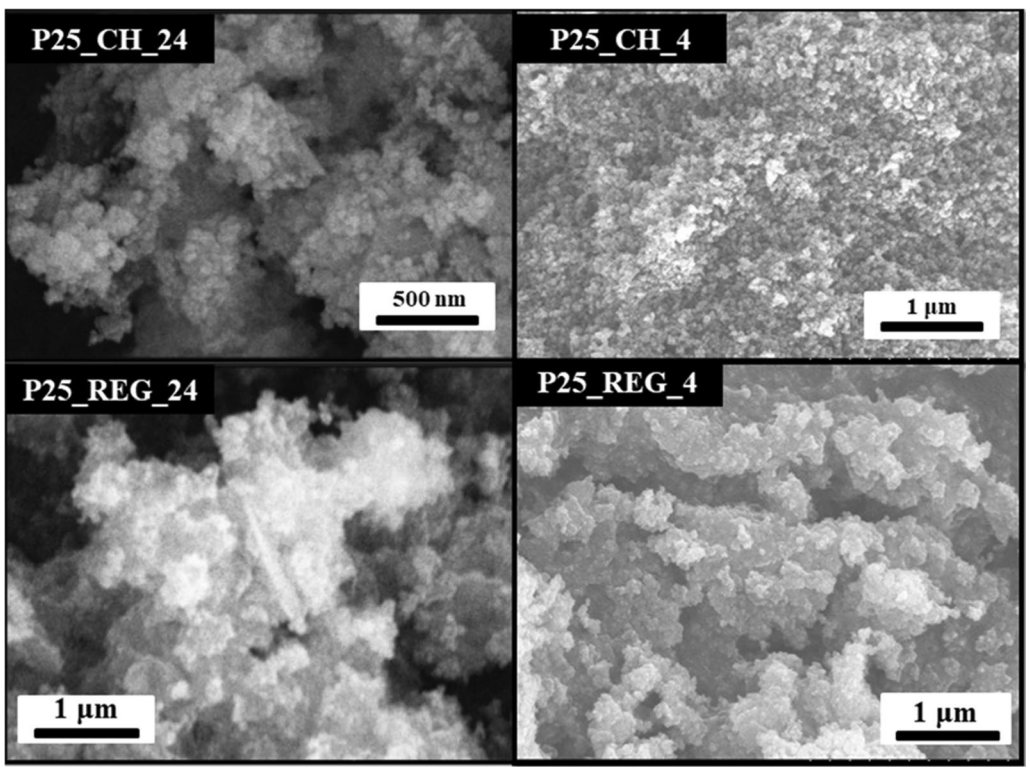

Fig. 4 SEM micrographs of P25 after interaction with the soil solutions

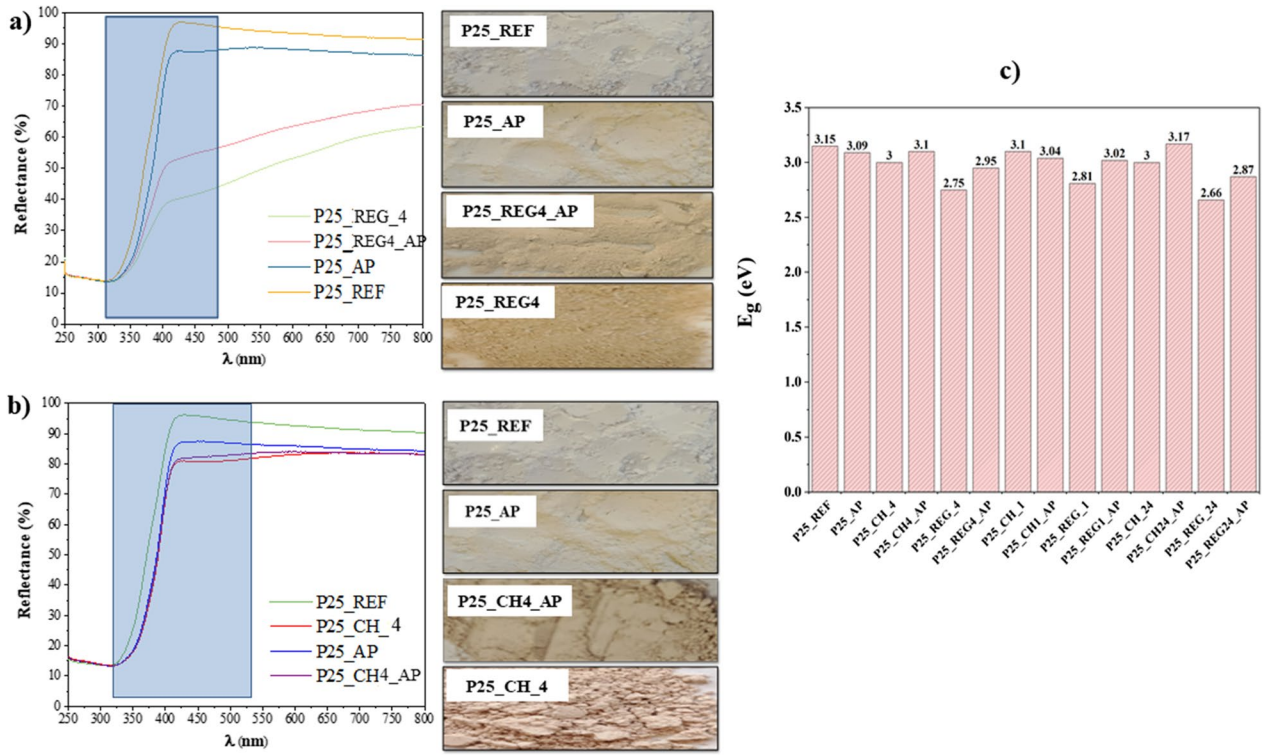

Fig. 5 DR spectra of the P25 samples and color changes before and after 4-h interaction with soil solutions: **a** Regosol soil solution, **b** Chernozem soil solution, **c** bandgap values of the samples

happens only through incorporation into the crystal lattice (doping) [64]. However, such a process cannot occur during adsorption, as it requires either a heat treatment or a hydrothermal process [65]. In contrast, various organic compounds, such as humic acids or conjugated double-bond-containing systems, can accept electrons (together with catalysts), causing bandgap changes [63]. Therefore, the significant color changes may have been caused by the surface-anchored organic compounds originating from the soil solutions, making the investigation of surface properties key to the present work.

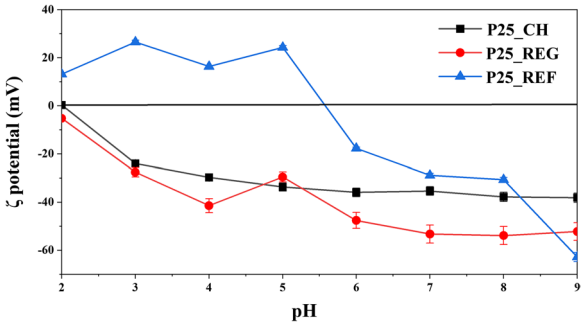

Fig. 6 ζ potential and IEP of P25 in distilled water, REG, and CH soil solutions

Surface properties of P25

Changes in the surface chemistry of P25 NPs were investigated by ζ potential measurements after their interaction with the soil solutions. This is because ζ potential plays a crucial role in the interaction of catalysts with each other or with other components (e.g., ions, organic compounds). ζ potential refers to the electrical charges on the surface of NPs in a solution, influencing stability and aggregation [26]. The ζ potential and IEP of P25 (Fig. 6) was investigated in REG, in CH, and, for comparability, in distilled water (P25_REF). The IEP refers to the pH at zero net total particle surface charge [66].

In distilled water, the IEP of P25 was ~ 5.65 pH units. However, the material's IEP in both soil solutions decreased to pH 2. This decrease is significant and indicates a substantial shift in the surface charge of the NPs. This may suggest, that a variety of dissolved ions, such as cations (Na^+ or Ca^{2+}) or organic species are present, which can adsorb onto the surface of the NPs and alter their surface charge. However, it is also possible that carboxyl groups from humic acids are adsorbed, which later on may suffer a deprotonation process.

The reason why the IEP did not change differently in the two soil solutions despite their differences in pH can be attributed to several factors. (i) The surface chemistry and composition of Evonik Aeroxide P25 NPs are primarily responsible for determining their isoelectric point. It is possible that the functional groups on the nanoparticle surface and their affinity to ionization remained consistent across the two soil solutions, leading to a similar shift in the IEP. (ii) Both acidic and slightly alkaline soil solutions can contain species that can protonate or deprotonate the functional groups on the nanoparticle surface, thereby affecting the surface charge. These species may be present in both soil solutions, leading to a similar change in the IEP.

Investigating the surface chemistry of nanomaterials in the aquatic environment using IR spectroscopy can provide valuable insights into their molecular interactions and surface functional groups. It allows the identification and characterization of adsorbed species, such as organic compounds or ions, which can influence the behavior of NPs.

As the next step, the IR spectra of the samples were recorded (Fig. 7, Additional file 1: Figs. S1, S2). Before analysis, it is important to clarify that the interaction time with the soil solutions did not influence the adsorption of various substances on the surface of the P25 NPs. Henceforth in the analysis, we will refer to the specific groups of samples as follows: those interacting with Chernozem soil solutions as P25_CH and P25_CH_AP, and those interacting with Regosols as P25_REG and P25_REG_AP.

Vibrations of Ti–O bonds in the 400–900 cm^{-1} region were detected. Since the P25 samples were not oxidized/reduced (due to the lack of conditions that enable such reactions), the IR spectra were normalized to the M–O (400–900 cm^{-1}) region.

Vibrations representative of CO_2 bonds at 2350 cm^{-1} was observed in all samples, originating from the sample preparation process and irrelevant to the analysis [67].

Bands at 1650 cm^{-1} were attributed to O–H bonds. This band was present not only in the samples exposed to soil solutions but in P25_REF too, which can be attributed to the presence of physisorbed water [68]. The intensity of this region varied in conjunction with that of the 3000–3500 cm^{-1} region ("water band") [69]. The intensity of the previous two regions did not change in parallel in our samples. If the intensity of these two regions does not increase in parallel, it suggests that a compound with additional O–H groups has been adsorbed onto the surface. In the P25_AP, P25_REG_AP, and P25_CH_AP samples, the significant changes between these regions could be attributed to the presence of phenol intermediates (e.g., hydroquinone, resorcinol, pyrocatechol) originating from the degradation process [7, 70, 71].

The bands identified so far were observed in each sample; however, differences in other regions were also observed and analyzed. In the 1600–1700 cm^{-1} region, bands with high intensities were observed in the P25_REG and P25_CH samples. These bands can be attributed to C=O and C=C vibrations originating from carboxyl groups (e.g., humic acids). In addition, N–H bonds were also detected in the 1580–1650 cm^{-1} region,

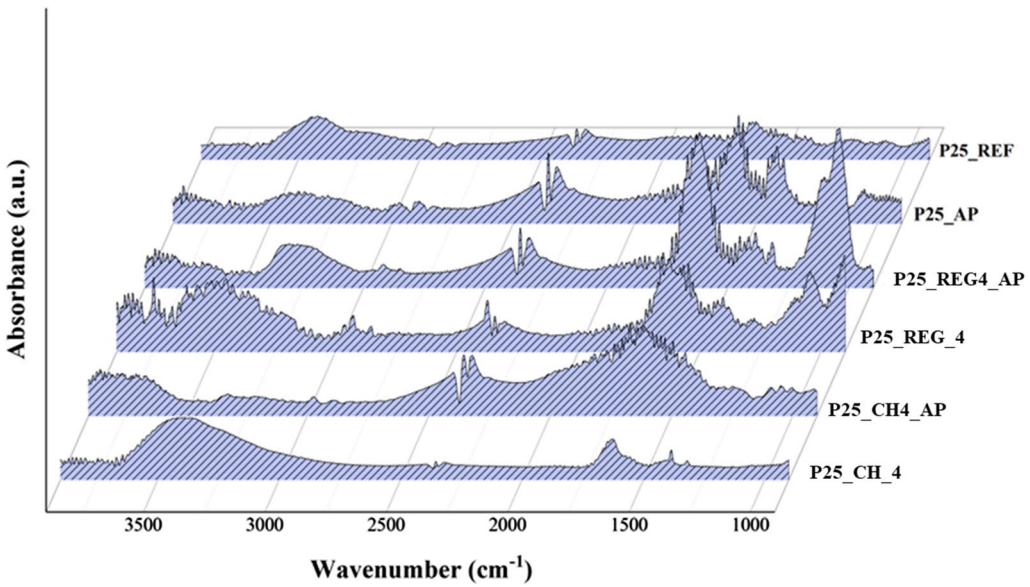

Fig. 7 IR spectra of the samples after 4-h interaction with the soil solutions in the 900–3900 cm^{-1} region

which may be attributed to different proteins/peptides from residues of animal and plant origins [72]. P25_CH, P25_REG, and P25_REG_AP had highly intensive bands in the 1000–1100 cm^{-1} region. These can mainly be attributed to Si–O bonds (1070–1030 cm^{-1}), since silicon oxides can be found in high amounts in the soil as inorganic compounds of different minerals [72]. In the same samples, C–O vibrations were also identified in the 1080–1100 cm^{-1} and 1250–1310 cm^{-1} regions, which can be ascribed to long carbon-chain molecules in soil solutions (e.g., lignin-based substances from the decomposition of plants [73]).

In the 1310–1380 cm^{-1} region, O–H bonds were observed in the P25_CH_AP, P25_REG_AP, and P25_AP samples, corresponding to the phenol degradation experiments. Another type of O–H bonds in the 1400–1420 cm^{-1} region could also be found in each sample, apart from P25_REF. For the P25_CH and P25_REG samples, this band may originate from the soil solutions (e.g., humic acid) [72], while in the other samples, this band may originate from the phenol degradation intermediates. Moreover, in the 1380–1390 cm^{-1} region, C–H bonds were identified, corresponding most likely to the aldehyde and alkaline groups of lignin in P25_CH and P25_REG [74]. However, it is worth noting that properly evaluating this region is challenging, because several vibrational bands overlap with each other. In P25_AP and P25_REG_AP, the intensive C=O bands in the 1690–1700 cm^{-1} region (aldehydes) also result from the phenol degradation experiments. Furthermore, intensive C=O bands were observed in the 1750–1820 cm^{-1} region in all samples except for P25_REF and P25_CH_AP [26]. Same as before, in this region, many vibrational bands overlap (e.g., aldehydes, carboxyl acids, esters, and anhydrides), which could originate from the phenol degradation process and the soil solutions. In the 2860–3000 cm^{-1} region, vibrations of C–H bonds were found with high intensity for P25_REG and P25_AP and with low intensity for P25_CH and P25_REG_AP [26].

Evaluation of photocatalytic activity after immersion in soil solution

The photocatalytic activity of P25 before and after its interaction with soil solutions was investigated via phenol degradation under UV-A light irradiation for 180 min. Previous adsorption studies have confirmed that the adsorption of phenol on P25 is negligible (~2–4%), so the adsorption–desorption equilibrium was reached in under 10 min.

As shown in Fig. 8, P25_REF degraded phenol completely after ~90 min. After its interaction with the CH, the activity decreased, and complete decomposition only occurred after 150 min regardless of the interaction time.

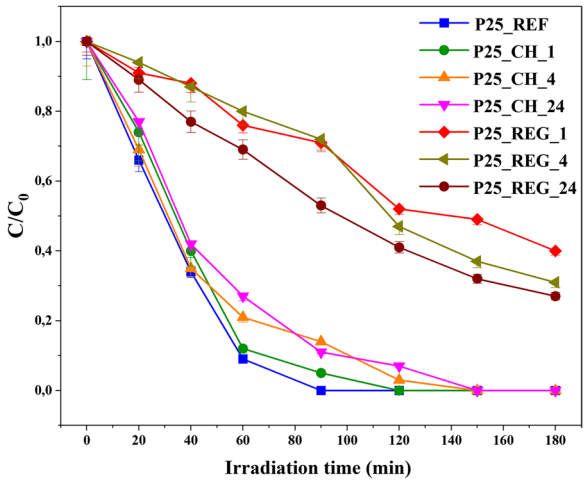

Fig. 8 Phenol degradation curves of P25 obtained before (P25_REF) and after its interaction with Regosol (P25_REG_1, 4, 24) and Chernozem (P25_CH_1, 4, 24) soil solutions

In contrast, after interacting with REG, the photocatalytic activity decreased drastically. For instance, in the case of P25_REG_1, only ~55% conversion was achieved after 180 min, while for P25_REG_4 and P25_REG_24, it was only about 60% and 62% respectively. It is clear that the cause for the decreasing photocatalytic activities must be related to the chemical compounds in the soil solutions. As discussed in the previous sections, P25 NPs underwent several changes after interacting with soil solutions.

In the P25_CH samples, no changes were observed in its morphological, structural, and semiconductive properties. However, as discussed in Sect. "Surface properties of P25", several organic compounds were adsorbed on the surface of the samples (e.g., carboxyl groups from humic acids, amines from pectines). Such organic compounds adsorbed on the surface can strongly influence photocatalytic activity in several ways. They can act as a physical barrier, reducing the surface area available for catalytic reactions by occupying active sites and undergoing degradation themselves instead of the target pollutant [49]. In addition, they can act as electron traps, decreasing the overall efficiency of photocatalysts. This effect is particularly significant for polar compounds, such as hydroxyl and carboxyl groups, which tend to adsorb onto the active surface of catalysts [75]. In addition, the CH solution had high F^-, Cl^-, and NO_3^- contents, and these ions can adsorb to the surface of P25, blocking active sites. F^- ions can form surface complexes with TiO_2, leading to surface passivation. This can reduce the availability of active sites, decrease the surface area available for adsorption, and decrease photocatalytic activity [55, 57, 59, 76, 77]. However, Na^+ concentration in the soil solution was also high, which can positively affect the activity

of P25. Na^+ can facilitate the adsorption of reactant molecules on the catalyst surface, promoting the availability of active sites for catalytic reactions [76].

After the interaction of P25 with the REG, aggregation, and bandgap changes were observed. These changes can be attributed to the high organic matter content of the REG (the REG had about eight times higher COD than the CH, as shown in Table 1). This statement is supported by the results presented in Sect. "Surface properties of P25", where it was described that several organic compounds were indeed adsorbed on the surface of the samples. However, as shown in Fig. 7, the intensity of each region in the IR spectrum is significantly higher than that after interaction with the CH. Besides the organic matter content, the acidic pH of the REG is important to consider. The positive surface charge of P25 in this pH range can influence the adsorption of various ions and consequently impede the accessibility of active sites [61]. This charge-related effect may contribute to the hindrance of adsorption and affect the overall efficiency of photocatalytic processes [78].

Conclusion

This study focused on investigating the properties of two different typed soil solutions and their effects on P25 TiO_2 NPs. Both soil solution induced aggregation of P25, reducing stability and promoting sedimentation. Optical changes were observed, but they may not significantly affect the photocatalytic properties of P25. The high organic matter content strongly affected the photocatalytic activity of P25, as organic compounds adsorbed onto its surface, hindering access to active sites. The investigation of inorganic ions in the soil solutions revealed notable differences in their concentrations, which influenced the ζ potential and aggregation of TiO_2 NPs. The evaluation of photocatalytic activity demonstrated that the presence of chemical compounds in the soil solutions affected the efficiency of P25. Organic compounds adsorbed on the surface acted as physical barriers and electron traps, reducing the availability of active sites and overall efficiency. In addition, inorganic ions could block active sites and decrease photocatalytic activity. Consideration of surface properties and the presence of various adsorbed compounds is essential for comprehending and optimizing the photocatalytic activity of NPs in soil environments. Our findings indicate that the duration of interaction did not exert a significant influence on the properties of TiO_2 NPs. However, chemical parameters, particularly the organic matter content, demonstrated a notable impact. This suggests that the behavior and characteristics of TiO_2 NPs are more strongly governed by the chemical composition of the environment they interact with rather than the duration of interaction. This highlights the stability of TiO_2 in the environment, emphasizing that its properties are more dependent on the chemical composition of the surroundings rather than the duration of interaction. Presently, despite their low concentrations, these materials demonstrate a high accumulation potential [79]. Most studies maintain TiO_2, including P25, to be inert and non-toxic upon environmental release. However, experimental results suggest an initial inhibition of TiO_2 activity, followed by an improvement over time. Notably, Chernozem exhibited comparable degradation efficiency to pure/reference P25 after interacting with soil solution. It is important to note that the best catalysts are UV-active and have a much higher quantum efficiency than visible light. At 3% UV light, UV catalysts can achieve a much higher degradation efficiency than a visible light-active catalyst in sunlight [80, 81]. This could potentially pose a significant environmental and ecological risk, as it continues to degrade the surrounding organic matter once released into the environment, consequently altering the chemical composition of the different environmental matrices, focused on the topsoil layers. Research has primarily focused on understanding how chemical parameters in soil/soil solution affect substance behavior. Future investigations will delve into reusability, and the influence of physical soil factors (e.g., texture) on TiO_2 behavior to enhance our comprehension of its environmental applicability and potential risks.

Supplementary Information

The online version contains supplementary material available at https://doi.org/10.1186/s12302-024-00903-y.

Additional file 1. Methodology and basic characterization of the soil solutions.

Acknowledgements

We express our gratitude to the landowners for allowing us entry to their individual farmlands. In addition, we recognize the contributions of Benjámin Pálffy, who assisted in the fieldwork throughout this study.

Author contributions

Karolina Solymos: conceptualization, investigation, writing–original draft, formal analysis. Izabella Babcsányi: conceptualization. Badam Ariya: investigation. Tamás Gyulavári: investigation, writing—review and editing. Áron Ágoston: investigation. Ákos Kukovecz: resources, funding acquisition. Zoltán Kónya: resources, funding acquisition. Zsolt Pap: conceptualization, visualization, writing—review and editing, supervision, funding acquisition.

Funding

Open access funding provided by University of Szeged. The authors would like to express their gratitude for the financial support provided by the 2019-2.1.13-TÉT_IN-2020-00015 project. T. Gyulavári is grateful for the financial support of the NKFI-PD-138248 project and the Bolyai János scholarship provided by the Hungarian Academy of Sciences (BO/00447/23). TKP2021-NVA-19 has been implemented with the support provided by the Ministry of Innovation and Technology of Hungary from the National Research, Development and Innovation Fund, financed under the TKP2021-NVA funding scheme.

Availability of data and materials
All data generated or analyzed during this study are included in this published article.

Declarations

Ethics approval and consent to participate
Not applicable.

Consent for publication
Not applicable.

Competing interests
The authors declare that they have no competing interest.

Received: 10 January 2024 Accepted: 7 April 2024
Published online: 25 April 2024

References

1. Ong W-J, Tan L-L, Chai S-P, Yong S-T, Mohamed AR (2014) Facet-dependent photocatalytic properties of TiO2-based composites for energy conversion and environmental remediation. Chemsuschem 7(3):690–719. https://doi.org/10.1002/cssc.201300924
2. Zaruma-Arias PE, Núñez-Núñez CM, González-Burciaga LA, Proal-Nájera JB (2022) Solar heterogenous photocatalytic degradation of methylthionine chloride on a flat plate reactor: effect of pH and H2O2 addition. Catalysts 12(2):132
3. Jiang X, Manawan M, Feng T, Qian R, Zhao T, Zhou G et al (2018) Anatase and rutile in evonik aeroxide P25: Heterojunctioned or individual nanoparticles? Catal Today 300:12–17. https://doi.org/10.1016/j.cattod.2017.06.010
4. Armaković SJ, Savanović MM, Armaković S (2023) Titanium dioxide as the most used photocatalyst for water purification: an overview. Catalysts 13(1):26
5. Kovács G, Fodor S, Vulpoi A, Schrantz K, Dombi A, Hernádi K et al (2015) Polyhedral Pt vs. spherical Pt nanoparticles on commercial titanias: Is shape tailoring a guarantee of achieving high activity? J Catal 325:156–167. https://doi.org/10.1016/j.jcat.2015.02.008
6. Kovács G, Baia L, Vulpoi A, Radu T, Karácsonyi É, Dombi A et al (2014) TiO2/WO3/Au nanoarchitectures' photocatalytic activity, "from degradation intermediates to catalysts' structural peculiarities", Part I: aeroxide P25 based composites. Appl Catal B 147:508–517. https://doi.org/10.1016/j.apcatb.2013.09.019
7. Gyulavári T, Pap Z, Kovács G, Baia L, Todea M, Hernádi K et al (2017) Peroxo group enhanced nanorutile as visible light active photocatalyst. Catal Today 284:129–136. https://doi.org/10.1016/j.cattod.2016.11.012
8. Alvear-Daza JJ, Pais-Ospina D, Marín-Silva DA, Pinotti A, Damonte L, Pizzio LR et al (2021) Facile photocatalytic immobilization strategy for P-25 TiO2 nanoparticles on low density polyethylene films and their UV-A photo-induced super hydrophilicity and photocatalytic activity. Catal Today 372:11–19. https://doi.org/10.1016/j.cattod.2020.07.029
9. Padmanabhan NT, John H (2020) Titanium dioxide based self-cleaning smart surfaces: a short review. J Environ Chem Eng 8(5):104211. https://doi.org/10.1016/j.jece.2020.104211
10. Hill D, Holliman PJ, McGettrick J, Searle J, Appelman M, Chatterjee P et al (2017) Studies of inherent lubricity coatings for low surface roughness galvanised steel for automotive applications. Lubr Sci 29(5):317–333. https://doi.org/10.1002/ls.1370
11. Mehregan S, Hayati F, Mehregan M, Isari AA, Jonidi Jafari A, Giannakis S et al (2022) Exploring the visible light–assisted conversion of CO2 into methane and methanol, using direct Z-scheme TiO2@g-C3N4 nanosheets: synthesis and photocatalytic performance. Environ Sci Pollut Res 29(49):74951–74966. https://doi.org/10.1007/s11356-022-21048-6
12. Zhu T, Cheng Y, Huang J, Xiong J, Ge M, Mao J et al (2020) A transparent superhydrophobic coating with mechanochemical robustness for anti-icing, photocatalysis and self-cleaning. Chem Eng J 399:125746. https://doi.org/10.1016/j.cej.2020.125746
13. Bundschuh M, Filser J, Lüderwald S, McKee MS, Metreveli G, Schaumann GE et al (2018) Nanoparticles in the environment: where do we come from, where do we go to? Environ Sci Eur 30(1):6. https://doi.org/10.1186/s12302-018-0132-6
14. Donia DT, Carbone M (2019) Fate of the nanoparticles in environmental cycles. Int J Environ Sci Technol 16(1):583–600. https://doi.org/10.1007/s13762-018-1960-z
15. Hochella MF, Mogk DW, Ranville J, Allen IC, Luther GW, Marr LC et al (2019) Natural, incidental, and engineered nanomaterials and their impacts on the Earth system. Science 363(6434):eaau8299. https://doi.org/10.1126/science.aau8299
16. Hu G, Cao J, Wang C, Lu M, Lin Z (2020) Study on the characteristics of naturally formed TiO2 nanoparticles in various surficial media from China. Chem Geol 550:119703. https://doi.org/10.1016/j.chemgeo.2020.119703
17. Nelson BC, Reipa V (2017) Analytical measurements of nanoparticles in challenging and complex environments. In Metrology and Standardization of Nanotechnology (pp. 175–196)
18. Meesters JAJ, Quik JTK, Koelmans AA, Hendriks AJ, van de Meent D (2016) Multimedia environmental fate and speciation of engineered nanoparticles: a probabilistic modeling approach. Environ Sci Nano 3(4):715–727. https://doi.org/10.1039/C6EN00081A
19. Luo Z-X, Wang Z-H, Xu B, Sarakiotis IL, Laing GD, Yan C-Z (2014) Measurement and characterization of engineered titanium dioxide nanoparticles in the environment. J Zhejiang Univ, Sci, A 15(8):593–605. https://doi.org/10.1631/jzus.A1400111
20. Johnson AC, Bowes MJ, Crossley A, Jarvie HP, Jurkschat K, Jürgens MD et al (2011) An assessment of the fate, behaviour and environmental risk associated with sunscreen TiO2 nanoparticles in UK field scenarios. Sci Total Environ 409(13):2503–2510. https://doi.org/10.1016/j.scitotenv.2011.03.040
21. Gottschalk F, Sonderer T, Scholz RW, Nowack B (2009) Modeled environmental concentrations of engineered nanomaterials (TiO2, ZnO, Ag, CNT, Fullerenes) for different regions. Environ Sci Technol 43(24):9216–9222. https://doi.org/10.1021/es9015553
22. Simonin M, Martins JMF, Uzu G, Spadini L, Navel A, Richaume A (2021) Low mobility of CuO and TiO2 nanoparticles in agricultural soils of contrasting texture and organic matter content. Sci Total Environ 783:146952. https://doi.org/10.1016/j.scitotenv.2021.146952
23. Nabi MM, Wang J, Baalousha M (2021) Episodic surges in titanium dioxide engineered particle concentrations in surface waters following rainfall events. Chemosphere 263:128261. https://doi.org/10.1016/j.chemosphere.2020.128261
24. Makselon J, Siebers N, Meier F, Vereecken H, Klumpp E (2018) Role of rain intensity and soil colloids in the retention of surfactant-stabilized silver nanoparticles in soil. Environ Pollut 238:1027–1034. https://doi.org/10.1016/j.envpol.2018.02.025
25. Gudkov SV, Shafeev GA, Glinushkin AP, Shkirin AV, Barmina EV, Rakov II et al (2020) Production and use of selenium nanoparticles as fertilizers. ACS Omega 5(28):17767–17774. https://doi.org/10.1021/acsomega.0c02448
26. Zehlike L, Peters A, Ellerbrock RH, Degenkolb L, Klitzke S (2019) Aggregation of TiO2 and Ag nanoparticles in soil solution—effects of primary nanoparticle size and dissolved organic matter characteristics. Sci Total Environ 688:288–298. https://doi.org/10.1016/j.scitotenv.2019.06.020
27. Rodrigues S, Bland GD, Gao X, Rodrigues SM, Lowry GV (2021) Investigation of pore water and soil extraction tests for characterizing the fate of poorly soluble metal-oxide nanoparticles. Chemosphere 267:128885. https://doi.org/10.1016/j.chemosphere.2020.128885
28. Tiwari E, Singh N, Khandelwal N, Ganie ZA, Choudhary A, Monikh FA et al (2022) Impact of nanoplastic debris on the stability and transport of metal oxide nanoparticles: role of varying soil solution chemistry. Chemosphere 308:136091. https://doi.org/10.1016/j.chemosphere.2022.136091
29. Galdames A, Ruiz-Rubio L, Orueta M, Sánchez-Arzalluz M, Vilas-Vilela JL (2020) Zero-valent iron nanoparticles for soil and groundwater remediation. Int J Environ Res Public Health. https://doi.org/10.3390/ijerph17165817
30. Sun H, Zhou S, Jiang Y, Xi X, Tan Y, Zhang G et al (2022) Chapter 7—fate and transport of engineered nanoparticles in soils and groundwater. In:

Gao B (ed) Emerging contaminants in soil and groundwater systems. Elsevier, pp 205–251
31. Degenkolb L, Kaupenjohann M, Klitzke S (2019) The variable fate of Ag and TiO2 nanoparticles in natural soil solutions—sorption of organic matter and nanoparticle stability. Water Air Soil Pollut 230(3):62. https://doi.org/10.1007/s11270-019-4123-z
32. Klitzke S, Metreveli G, Peters A, Schaumann GE, Lang F (2015) The fate of silver nanoparticles in soil solution—sorption of solutes and aggregation. Sci Total Environ 535:54–60. https://doi.org/10.1016/j.scitotenv.2014.10.108
33. Qiu Y, Mu Z, Wang N, Wang X, Xu M, Li H (2020) The aggregation and sedimentation of two different sized copper oxide nanoparticles in soil solutions: dependence on pH and dissolved organic matter. Sci Total Environ 731:139215. https://doi.org/10.1016/j.scitotenv.2020.139215
34. Xu M, Wang Y, Mu Z, Li S, Li H (2021) Dissolution of copper oxide nanoparticles is controlled by soil solution pH, dissolved organic matter, and particle specific surface area. Sci Total Environ 772:145477. https://doi.org/10.1016/j.scitotenv.2021.145477
35. Eckmeier E, Gerlach R, Gehrt E, Schmidt MWI (2007) Pedogenesis of Chernozems in Central Europe—a review. Geoderma 139(3):288–299. https://doi.org/10.1016/j.geoderma.2007.01.009
36. Lucian R, Nicolae G, Mărăcineanu L (2021) The analysis of physical and chemical properties of Regosol from Brădești, Dolj county. XXV (LXI), 190–195
37. Uvarov V, Popov I (2007) Metrological characterization of X-ray diffraction methods for determination of crystallite size in nano-scale materials. Mater Charact 58(10):883–891. https://doi.org/10.1016/j.matchar.2006.09.002
38. Tunc I, Bruns M, Gliemann H, Grunze M, Koelsch P (2010) Bandgap determination and charge separation in Ag@TiO2 core shell nanoparticle films. Surf Interface Anal 42(6–7):835–841. https://doi.org/10.1002/sia.3558
39. Shih YH, Liu WS, Su YF (2012) Aggregation of stabilized TiO2 nanoparticle suspensions in the presence of inorganic ions. Environ Toxicol Chem 31(8):1693–1698. https://doi.org/10.1002/etc.1898
40. Fu PP, Xia Q, Hwang HM, Ray PC, Yu H (2014) Mechanisms of nanotoxicity: generation of reactive oxygen species. J Food Drug Anal 22(1):64–75. https://doi.org/10.1016/j.jfda.2014.01.005
41. Skocaj M, Filipic M, Petkovic J, Novak S (2011) Titanium dioxide in our everyday life; is it safe? Radiol Oncol 45(4):227–247. https://doi.org/10.2478/v10019-011-0037-0
42. Czekes Z, Bai D, Vincze J, Gál E, Réthi-Nagy Z, Baia L et al (2023) Commercial photocatalyst changes the behavior of Formica pratensis and Formica polyctena. Environ Sci Nano 10(1):72–79. https://doi.org/10.1039/D1EN01119G
43. Selvakesavan RK, Kruszka D, Shakya P, Mondal D, Franklin G (2023) Impact of nanomaterials on plant secondary metabolism. In: Al-Khayri JM, Alnaddaf LM, Jain SM (eds) Nanomaterial interactions with plant cellular mechanisms and macromolecules and agricultural implications. Springer International Publishing, Cham, pp 133–170
44. Coutts J, Hintze P, Meier A, Devor R, Surma J, Maloney P, et al (2016) Visible-light-responsive photocatalysis: Ag-doped TiO2 catalyst development and reactor design testing
45. Holm A, Hamandi M, Simonet F, Jouguet B, Dappozze F, Guillard C (2019) Impact of rutile and anatase phase on the photocatalytic decomposition of lactic acid. Appl Catal B 253:96–104. https://doi.org/10.1016/j.apcatb.2019.04.042
46. Ishigaki T, Nakada Y, Tarutani N, Uchikoshi T, Tsujimoto Y, Isobe M et al (2020) Enhanced visible-light photocatalytic activity of anatase-rutile mixed-phase nano-size powder given by high-temperature heat treatment. R Soc Open Sci 7(1):191539. https://doi.org/10.1098/rsos.191539
47. Wang K, Wei Z, Colbeau-Justin C, Nitta A, Kowalska E (2022) P25 and its components—electronic properties and photocatalytic activities. Surf Interfaces 31:102057. https://doi.org/10.1016/j.surfin.2022.102057
48. Ontman R, Groffman PM, Driscoll CT, Cheng Z (2023) Surprising relationships between soil pH and microbial biomass and activity in a northern hardwood forest. Biogeochemistry 163(3):265–277. https://doi.org/10.1007/s10533-023-01031-0
49. Fattahi A, Arlos MJ, Bragg LM, Liang R, Zhou N, Servos MR (2021) Degradation of natural organic matter using Ag-P25 photocatalyst under continuous and periodic irradiation of 405 and 365 nm UV-LEDs. J Environ Chem Eng 9(1):104844. https://doi.org/10.1016/j.jece.2020.104844
50. Pavel M, Anastasescu C, State R-N, Vasile A, Papa F, Balint I (2023) Photocatalytic degradation of organic and inorganic pollutants to harmless end products: assessment of practical application potential for water and air cleaning. Catalysts 13(2):380
51. French RA, Jacobson AR, Kim B, Isley SL, Penn RL, Baveye PC (2009) Influence of ionic strength, pH, and cation valence on aggregation kinetics of titanium dioxide nanoparticles. Environ Sci Technol 43(5):1354–1359. https://doi.org/10.1021/es802628n
52. Tran ML, Fu C-C, Juang R-S (2019) Effects of water matrix components on degradation efficiency and pathways of antibiotic metronidazole by UV/TiO2 photocatalysis. J Mol Liq 276:32–38. https://doi.org/10.1016/j.molliq.2018.11.155
53. He H, Cheng Y, Yang C, Zeng G, Zhu C, Yan Z (2017) Influences of anion concentration and valence on dispersion and aggregation of titanium dioxide nanoparticles in aqueous solutions. J Environ Sci 54:135–141. https://doi.org/10.1016/j.jes.2016.06.009
54. Zhao D, Chen C, Wang Y, Ji H, Ma W, Zang L et al (2008) Surface modification of TiO2 by phosphate: effect on photocatalytic activity and mechanism implication. J Phys Chem C 112(15):5993–6001. https://doi.org/10.1021/jp712049c
55. Watanabe Y, Tait K, Gregory S, Hayashi M, Shimamoto A, Taylor P et al (2015) Response of the ammonia oxidation activity of microorganisms in surface sediment to a controlled sub-seabed release of CO2. Int J Greenhouse Gas Control 38:162–170. https://doi.org/10.1016/j.ijggc.2014.11.013
56. Gong X, Wang H, Yang C, Li Q, Chen X, Hu J (2015) Photocatalytic degradation of high ammonia concentration wastewater by TiO2. Future Cities Environ 1(1):12. https://doi.org/10.1186/s40984-015-0012-9
57. Zhao J, Liu S, Zhang X, Xu Y (2020) Different effects of fluoride and phosphate anions on TiO2 photocatalysis (rutile). Catal Sci Technol 10(19):6552–6561. https://doi.org/10.1039/D0CY01111H
58. Zhang J, Wang X, Wang J, Wang J, Ji Z (2016) Effect of sulfate ions on the crystallization and photocatalytic activity of TiO2/diatomite composite photocatalyst. Chem Phys Lett 643:53–60. https://doi.org/10.1016/j.cplett.2015.11.020
59. Delarmelina M, Dlamini MW, Pattisson S, Davies PR, Hutchings GJ, Catlow CRA (2023) The effect of dissolved chlorides on the photocatalytic degradation properties of titania in wastewater treatment. Phys Chem 25(5):4161–4176. https://doi.org/10.1039/D2CP03140J
60. Colón G, Hidalgo MC, Navio JA (2003) Photocatalytic behaviour of sulphated TiO2 for phenol degradation. Appl Catal B 45(1):39–50. https://doi.org/10.1016/S0926-3373(03)00125-5
61. Luo M, Huang Y, Zhu M, Tang Y-N, Ren T, Ren J et al (2018) Properties of different natural organic matter influence the adsorption and aggregation behavior of TiO2 nanoparticles. J Saudi Chem Soc 22(2):146–154. https://doi.org/10.1016/j.jscs.2016.01.007
62. Danielsson K, Gallego-Urrea JA, Hassellov M, Gustafsson S, Jonsson CM (2017) Influence of organic molecules on the aggregation of TiO(2) nanoparticles in acidic conditions. J Nanopart Res 19(4):133. https://doi.org/10.1007/s11051-017-3807-9
63. Pap Z, Mogyorósi K, Veréb G, Dombi A, Hernádi K, Danciu V et al (2014) Commercial and home-made nitrogen modified titanias. A short reflection about the advantageous/disadvantageous properties of nitrogen doping in the frame of their applicability. J Mol Struct 1073:157–163. https://doi.org/10.1016/j.molstruc.2014.05.023
64. Apostolova I, Apostolov A, Wesselinowa J (2022) Band gap tuning in transition metal and rare-earth-ion-doped TiO(2), CeO(2), and SnO(2) nanoparticles. Nanomaterials (Basel). https://doi.org/10.3390/nano13010145
65. Lertthanaphol N, Pienutsa N, Chusri K, Sornsuchat T, Chanthara P, Seeharaj P et al (2021) One-step hydrothermal synthesis of precious metal-doped titanium dioxide-graphene oxide composites for photocatalytic conversion of CO2 to ethanol. ACS Omega 6(51):35769–35779. https://doi.org/10.1021/acsomega.1c05799
66. Suttiponparnit K, Jiang J, Sahu M, Suvachittanont S, Charinpanitkul T, Biswas P (2010) Role of surface area, primary particle size, and crystal phase on titanium dioxide nanoparticle dispersion properties. Nanoscale Res Lett 6(1):27. https://doi.org/10.1007/s11671-010-9772-1
67. Iskra A, Gentleman AS, Kartouzian A, Kent MJ, Sharp AP, Mackenzie SR (2017) Infrared spectroscopy of gas-phase M+(CO2)n (M = Co, Rh, Ir)

ion-molecule complexes. J Phys Chem A 121(1):133–140. https://doi.org/10.1021/acs.jpca.6b10902
68. Khatib R, Backus EHG, Bonn M, Perez-Haro M-J, Gaigeot M-P, Sulpizi M (2016) Water orientation and hydrogen-bond structure at the fluorite/water interface. Sci Rep 6(1):24287. https://doi.org/10.1038/srep24287
69. van der Post ST, Hsieh C-S, Okuno M, Nagata Y, Bakker HJ, Bonn M et al (2015) Strong frequency dependence of vibrational relaxation in bulk and surface water reveals sub-picosecond structural heterogeneity. Nat Commun 6(1):8384. https://doi.org/10.1038/ncomms9384
70. Vardar G, Wood TK (2004) Protein engineering of toluene-o-xylene monooxygenase from *Pseudomonas stutzeri* OX1 for synthesizing 4-methylresorcinol, methylhydroquinone, and pyrogallol. Appl Environ Microbiol 70(6):3253–3262. https://doi.org/10.1128/AEM.70.6.3253-3262.2004
71. Gyulavári T, Veréb G, Pap Z, Réti B, Baan K, Todea M et al (2019) Utilization of carbon nanospheres in photocatalyst production: from composites to highly active hollow structures. Materials 12(16):2537
72. Machado W, Franchini JC, de Fátima Guimarães M, Filho JT (2020) Spectroscopic characterization of humic and fulvic acids in soil aggregates, Brazil. Heliyon 6(6):e04078. https://doi.org/10.1016/j.heliyon.2020.e04078
73. da Silva AP, Babujia LC, Franchini JC, Ralisch R, Hungria M, de Guimarães MF (2014) Soil structure and its influence on microbial biomass in different soil and crop management systems. Soil Tillage Res 142:42–53. https://doi.org/10.1016/j.still.2014.04.006
74. Hong Y, Chen S, Liu Y, Zhang Y, Yu L, Chen Y et al (2019) Combination of fractional order derivative and memory-based learning algorithm to improve the estimation accuracy of soil organic matter by visible and near-infrared spectroscopy. CATENA 174:104–116. https://doi.org/10.1016/j.catena.2018.10.051
75. Mathew RA, Wu G, Zhang Y, Shakiba S, Yao Y, Tsai A-L et al (2021) Natural organic matter adsorption conditions influence photocatalytic reaction pathways of phosphate-treated titanium dioxide nanoparticles. Environ Sci Nano 8(8):2165–2176. https://doi.org/10.1039/D1EN00433F
76. Abdullah M, Low GKC, Matthews RW (1990) Effects of common inorganic anions on rates of photocatalytic oxidation of organic carbon over illuminated titanium dioxide. J Phys Chem 94(17):6820–6825. https://doi.org/10.1021/j100380a051
77. Solymos K, Babcsányi I, Ariya B, Gyulavári T, Ágoston Á, Szamosvölgyi Á et al (2024) Photocatalytic and surface properties of titanium dioxide nanoparticles in soil solutions. Environ Sci Nano. https://doi.org/10.1039/D3EN00622K
78. Sapińska D, Adamek E, Masternak E, Zielińska-Danch W, Baran W (2022) Influence of pH on the kinetics and products of photocatalytic degradation of sulfonamides in aqueous solutions. Toxics 10(11):655
79. Shah SNA, Shah Z, Hussain M, Khan M (2017) Hazardous effects of titanium dioxide nanoparticles in ecosystem. Bioinorg Chem Appl 2017:4101735. https://doi.org/10.1155/2017/4101735
80. Ge Y, Luo H, Huang J, Zhang Z (2021) Visible-light-active TiO2 photocatalyst for efficient photodegradation of organic dyes. Opt Mater 115:111058. https://doi.org/10.1016/j.optmat.2021.111058
81. Haider AJ, Al-Anbari RH, Kadhim GR, Salame CT (2017) Exploring potential Environmental applications of TiO2 Nanoparticles. Energy Procedia 119:332–345. https://doi.org/10.1016/j.egypro.2017.07.117

Publisher's Note